Proceedings of the
Annual Stability Conference
Structural Stability Research Council
Louisville, Kentucky, April 13-16, 2021

Influence of perforation pattern in Direct Strength Method of upright design

J Vijaya Vengadesh Kumar[1], Ashish Gupta[2], Harisanth K S[3] S Arul Jayachandran[4]

Abstract

The Direct Strength Method design of thin-walled cold-formed steel members is recently extended to perforated members and implemented in AISI-2016 specification. Albeit the background research is well constructed for discrete perforations, it requires more attention to pattern perforations. Perhaps the range of upright cross-sections and perforation shapes available in the market are patented, is the main reason for the lack of experimental data in this research domain. Available literature reports a pool of numerical data resulting from finite element analysis accounting the parameters such as cross-section shape, thickness, perforation shape, the spacing between perforations, member lengths, etc. These numerical models are mainly calibrated with the experimental results of fixed end columns. It should be noted that the fixed end columns are not influenced by the shift of effective centroid. Using such results in developing analytical equations will end up with the ignorance of effective centroid shift. The systematic experiments on perforated compression members in the view of simply supported boundary conditions are scarce. Therefore, experimental results with respect to flexural boundary conditions are reported herein. With the results of experiments, the influence of perforations is rationally assessed for local, distortional and flexural buckling about minor axis. The interaction between the modes is also observed and reported. The DSM design procedure recommended in the AISI-2016 is validated with the experimental results and summarized for the safe and economic design of uprights.

1. Introduction

Thin-walled cold-formed steel sections are popular due to their high strength to weight ratio, ease in fabrication and erection. Thus, the cold-formed steel is optimally engineered as various structural members in the industrial storage rack structures. The upright members are the predominant compression members in the rack system which has pattern perforations along the member length to enable the beam connection with upright frames at desired heights. These uprights are formed by rolling the thin sheets and resulting in open cross-section with one axis of symmetry. The mono-symmetry, open cross-section nature and, perforations along the member length render the design complications. In particular, the mono-symmetry is related to the possibility of flexural-torsional mode, the open cross-section has the lower torsional resistance and also provides room for distortional mode, and further the perforations can significantly reduce the strength (Rhodes and Schneider 1994 and Rhodes and Macdonald 1996). The

[1] Assistant Professor, National Institute of Technology Karnataka - India, <vj@nitk.edu.in>
[2] Post-Graduate Student, National Institute of Technology Karnataka - India, <profemailname@superduper.edu>
[3] Post-Graduate Student, Indian Institute of Technology Madras - India, <harisanthks92@gmail.com>
[4] Professor, Indian Institute of Technology Madras - India, <aruls@iitm.ac.in>

complex stiffeners, flange perforations, upright frame bracing types, connection rigidity, patented cross-section shapes, and perforations add additional complexity in the design of uprights. Since the cross-sections and perforation patterns are patented by the manufacturers the experimental results on uprights are scarce and even the available results are not reproducible using finite element analysis due to masking of necessary data (Davies et. al. 1997, Casafont et. al. 2011, Rouri et. al. 2011, Trouncer and Rasmuseen (2014a and b), Kumar and Jayachandran 2016 and Baldassino et. al. 2019). Therefore, the storage rack design codes (EN 15512:2009 and RMI: 2012) prescribe the experiments-based design to capture the behavior as close as to the real behavior of uprights. Nevertheless, this experiments-based design is expensive, laborious, and time-consuming.

Effective Width Method (EWM) of design for uprights is complex in determining the effective section properties for cross-sections having multiple stiffeners and perforations and the presence of bending moment if any, results in iterative design (Yu and LaBoube 2010). However, the computer-aided design of compression members using Direct Strength Method (DSM) is simple and straight forward for any complex geometry (AISI S100:2016). The main advantages of DSM are non-iterative, local buckling accounts the inter element interactions, minimum local, distortional and global elastic critical buckling loads can be determined from the signature curve plotted for the ratio of elastic critical buckling stress to applied stress in vertical axis and half wavelength in horizontal axis. Signature curve systematically accounts for all possible half wavelengths within member length. This semi-empirical method is proven as a reliable design method for cross-sections with or without discrete perforations (Moen 2008, Moen and Schafer 2008, Moen and Schafer 2009 and Moen and Schafer 2011). Discrete perforations are accounted in terms of reduced element thickness for the strip having perforations. Reduced thickness equations are well calibrated with large number of experimental and numerical analysis results. Albeit the same reduced thickness approach is proposed for the pattern perforations (Casafont et. al. 2013 and Smith and Moen 2014), those equations are calibrated with the exciting limited experimental results and numerical results. Lack of experimental results for pattern perforations hinders the researchers to develop the more accurate reduced thickness equations. It should be noted that the effective shift in centroid of cross-section due to buckling and perforations will not create any additional moments for fixed support columns whereas it may be significant for the simply supported conditions (Young and Rasmuseen 1998). Unfortunately, the experimental results are mostly available for fixed boundary conditions with less attention to simply supported boundary conditions. Moreover, the DSM design does not account for effective centroid shift.

This article addresses the behavior of simple rack uprights flexurally simply supported about the minor principal axis subject to axial compression in the presence of idealized perforation patterns along member length. The systematic experimental results for various member lengths for unperforated, and perforations of rectangle and square shapes are presented. Finally, the results are compared with the DSM design prediction presented in literature by the researchers for pattern perforations and conclusions are drawn.

2. Experimental Study

The geometry of the cross-section for the experiments were decided based on number of signature curves (for half wavelengths) and elastic critical buckling curves (for actual member lengths) determined using CUFSM software (Schafer and Adany 2006 and Li and Schafer 2010)

considering the parameters of height to width ratio, flange to rear flange ratio and flange stiffener length. The uprights available in the market are having the height to width ratio ranges in between 1.2 and 1.5. Based on elastic critical buckling analysis, the cross-section having height to width ratio of 1.3 which has nearly equal elastic critical buckling load for local and distortional modes, was considered in this study. The finalized cross-section dimensions are 80×40×20×15×1.6 mm respectively the height, flange width, rear flange width, flange stiffener length and thickness of the section. The inter elements of cross-section are bent orthogonally to form a simple rack section as shown in Fig.1(a).

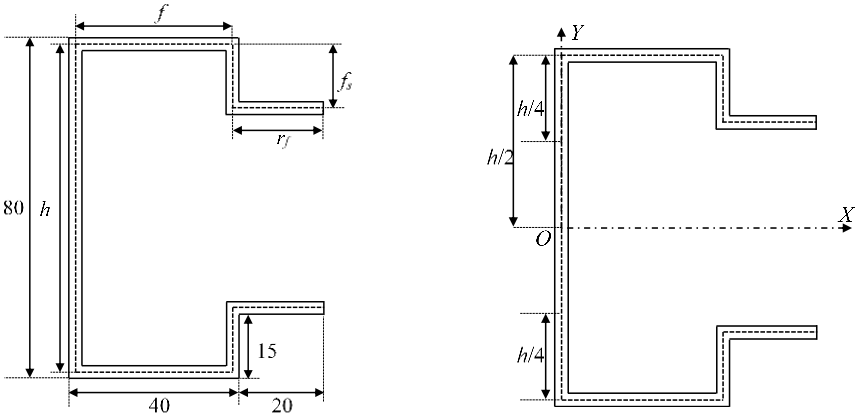

Figure 1: Simple Rack Section

The unperforated member is considered as the controlling specimen and two web perforation patterns of rectangle and square shapes are calibrated in this study. Two numbers of perforations are considered in the transverse direction of web element and the center of the perforation is located at the center of half web element above and below the symmetry axis as shown in Fig.1(b). The area of square perforation is double the times area of rectangular perforation. Perforation pattern P1 has the dimension of 10×20 mm respectively along transverse and longitudinal direction, whereas P3 perforation dimension is 20×20 mm. The member lengths are carefully chosen to get the possible interaction of distortional mode with local and/ or global minor axis flexural mode. In total, five lengths are considered and the lengths are in proportion to overall web depth of the section. The knife edge supports are provided at both the ends to enable the flexural buckling about minor axis. However, the flexural buckling about major axis, local, distortional modes, warping and twisting about longitudinal axis are restrained at the ends. Mono-symmetry section failing in global mode will be governed by the minimum of flexural buckling about minor axis or flexural-torsional buckling. The upright sections used in storage racks are generally mono-symmetric and braced in its upright frame. Depending on this bracing pattern, the effective length for flexural buckling and flexural-torsional buckling will be considerably different. Thus, the upright may fail in minor axis flexural mode which brings the direct relevance to this experimental study.

The hot-rolled sheets are press braked to form the simple rack section and before forming, the perforations are cut using precise laser cut technology. The internal corner radius of the section was maintained equal to nominal thickness of the sheet and hence, reasonably treated as sharp edges in all the calculations and modelling of cross-section. The dimensions of the fabricated

sections were measured at three locations along the member length at equal interval, however the symmetry is presumed and the average of the measured element lengths are considered in the study. The complete geometrical properties of the sections using the average of measured values are presented in the Table1 to Table 3. Specimen lengths are referred as L1 to L5 with respect to its effective length, as presented in Table 1. In which the letter following effective length means the perforation type. For example, L1G represents the member has nominal effective length of 580 mm and the member is unperforated and thus G is used for gross (unperforated) section. The Table 1 shows the centerline dimensions of every plate element determined using measured values as shown in Fig. 1(a). The geometrical properties for the measured cross-section are calculated and presented in Table 2 for gross section and Table 3 for net section having perforations. The material properties of yield stress and Young's modulus were determined form the coupon tests as 255 N/mm^2 and 2×10^5 N/mm^2.

Table 1: Measured geometrical dimensions

Name	L (mm)	h (mm)	f (mm)	r_f (mm)	f_s (mm)	t (mm)
L1G	579	77.95	38.66	20.65	14.89	1.59
L2G	819	77.93	38.39	20.73	15.10	1.60
L3G	1059	77.89	38.63	20.81	15.09	1.60
L4G	1300	77.84	38.62	20.77	14.97	1.60
L5G	1540	78.02	38.92	21.01	14.77	1.59
L1P1	579	78.31	38.98	20.74	15.05	1.60
L2P1	819	77.85	39.07	20.81	15.06	1.56
L3P1	1060	77.65	38.84	20.89	14.88	1.59
L4P1	1299	78.04	38.54	20.87	15.36	1.59
L5P1	1539	78.23	38.86	20.84	14.92	1.59
L1P3	579	77.98	39.02	20.64	14.92	1.61
L2P3	819	78.42	38.57	20.69	14.95	1.61
L3P3	1060	78.17	38.93	20.76	14.85	1.59
L4P3	1300	77.98	38.53	20.88	14.93	1.59
L5P3	1539	78.14	39.23	20.98	14.81	1.60

Table 2: Gross section properties

Name	A (mm^2)	X_{cg} (mm)	Y_{cg} (mm)	I_1 $\times10^3$ (mm^4)	I_2 $\times10^3$ (mm^4)	J (mm^4)	X_o (mm)	Y_o (mm)	C_w $\times10^6$ (mm^6)	β_1	β_2
L1G	360.62	20.62	0.00	336.27	139.07	305.17	50.25	0.00	310.94	0.00	109.39
L2G	362.37	20.56	0.00	336.23	138.62	309.48	50.13	0.00	313.01	0.00	108.88
L3G	363.88	20.71	0.00	337.68	140.75	311.80	50.44	0.00	317.69	0.00	109.47
L4G	361.57	20.67	0.00	335.64	139.66	307.00	50.36	0.00	313.05	0.00	109.43
L5G	362.33	20.85	0.00	339.07	142.46	306.62	50.74	0.00	317.33	0.00	110.43
L1P1	365.33	20.80	0.00	343.64	142.96	313.05	50.68	0.00	324.37	0.00	110.17
L2P1	355.37	20.91	0.00	330.40	139.77	288.42	50.91	0.00	315.41	0.00	110.39
L3P1	360.96	20.82	0.00	334.03	141.03	304.57	50.68	0.00	314.33	0.00	110.04
L4P1	362.09	20.71	0.00	335.97	139.76	305.51	50.48	0.00	320.36	0.00	109.29
L5P1	361.37	20.76	0.00	339.47	141.12	304.01	50.58	0.00	317.62	0.00	110.07
L1P3	365.09	20.79	0.00	341.26	142.69	314.40	50.64	0.00	320.21	0.00	110.12
L2P3	364.67	20.56	0.00	343.76	140.32	314.18	50.13	0.00	316.70	0.00	109.30
L3P3	362.39	20.77	0.00	340.45	141.66	307.18	50.58	0.00	317.41	0.00	110.15
L4P3	360.57	20.65	0.00	335.78	139.24	304.11	50.31	0.00	312.12	0.00	109.42
L5P3	365.19	20.98	0.00	343.22	145.17	311.76	51.06	0.00	325.10	0.00	111.04

Table 3: Net section properties

Name	A	X_{cg}	Y_{cg}	I_1 $\times 10^3$	I_2 $\times 10^3$	J	X_o	Y_o	C_w $\times 10^6$	β_1	β_2
	(mm^2)	(mm)	(mm)	(mm^4)	(mm^4)	(mm^4)	(mm)	(mm)	(mm^6)		
L1P1	333.26	22.81	0.00	331.09	127.74	285.57	53.81	0.00	312.74	0.00	110.58
L2P1	324.16	22.93	0.00	318.31	124.79	263.09	54.06	0.00	304.13	0.00	110.84
L3P1	329.14	22.83	0.00	321.77	125.89	277.72	53.83	0.00	302.99	0.00	110.48
L4P1	330.27	22.71	0.00	323.59	124.78	278.67	53.62	0.00	308.97	0.00	109.69
L5P1	329.59	22.77	0.00	327.05	126.09	277.28	53.71	0.00	306.16	0.00	110.48
L1P3	300.80	25.24	0.00	314.68	108.93	259.04	57.60	0.00	294.54	0.00	110.75
L2P3	300.37	24.96	0.00	316.90	107.29	258.78	57.04	0.00	291.22	0.00	109.80
L3P3	298.61	25.20	0.00	313.96	108.26	253.12	57.53	0.00	291.89	0.00	110.77
L4P3	296.94	25.08	0.00	309.48	106.28	250.45	57.26	0.00	287.01	0.00	110.02
L5P3	301.18	25.44	0.00	316.66	110.98	257.11	58.04	0.00	299.07	0.00	111.76

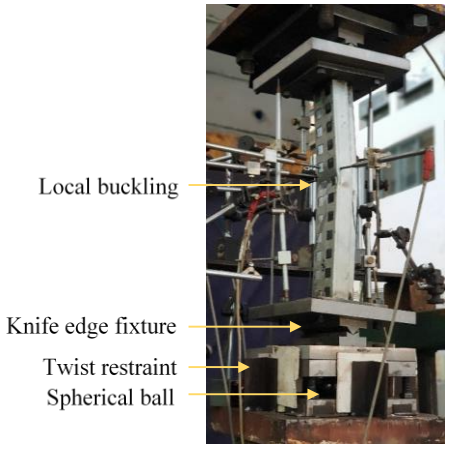

Figure 2: Experimental setup

Figure 3: Failure mode of L1 and L4 specimens

The specimens were carefully arc welded at both the ends with the mild steel square plates of dimension 170×170×10 mm, in such a way that the centroid of gross section matches with centroid of the end plates. The weld distortions were avoided by systematic non-continuous

stitch welding. These end plates were bolted with the knife edge support plates and the resulting knife edge to knife edge distance is the effective length for flexural buckling about the minor axis. The experimental setup is presented in Fig. 3. Once the specimen is placed between the knife edges, a preload of 0.5 kN was applied using the actuator and the special bearing below the bottom knife edge is brought into action by releasing the four corner bolts preventing the rotation of the bottom knife edge plate about both the axes. This spherical bearing allows the finer alignment of the specimen and the straightness of the specimen is assured using laser alignment device, in two perpendicular directions. In the aligned position, the spherical bearing is locked using the bolts by making it to touch the bottom knife edge plate. The displacement-controlled load was increased at the rate of 1 mm per minute. The axial shortening, rotation about minor axis, deflection and rotation of cross-section at mid length were recorded using displacement transducers (LVDT) and load from load cell using data acquisition system at the rate of 5 readings per second. Three strain gauges were attached in flange and rear flanges at mid length to monitor the strain readings. The loading was continued until there was a reduction in forty percent of ultimate failure load. The ultimate failure load for all members is presented in Table 4 and the failure modes for representative specimens are shown in Fig. 3. These ultimate failure loads for simply supported about minor principal axis may be smaller than that of fixed support column having same effective length, due to the shift in effective centroid along the symmetry axis. The secondary bending moment due to shift in effective centroid is automatically balanced by the fixed supports however, it lowers the ultimate capacity of specimens flexurally simply supported about minor axis. This effective centroid shift is mainly attributed with local buckling but, it is further boosted in uprights due to the perforations along the member length which implying the varying centroid for gross and net cross-sections even before local buckling. Therefore, the presented experimental results are relatively conservative in estimating the ultimate failure load by inherently including effective centroid shift.

3. Direct Strength Method of Design

At present, the upright members are designed as per the experiments recommended in code provisions to include all possible uncertainties and to closely relate the design with actual rack behavior. Despite the code permits the finite element analysis to design the upright members, its admissibility is depending on the accuracy of user inputs for geometrical and material modelling, mesh convergence and assumptions made in the analysis. Since it requires commercial software and high-end computational facilities, it may be uneconomic and the accuracy of the results are subjective. The analytical based design strength estimation can be a quick reference for the designers to arrive initial geometry of conceptual design. The upright sections are highly suspectable to local buckling and hence Effective Width Method (EWM) or Direct Strength Method (DSM) are the suitable design methods. Among these two methods, DSM is the best suitable design method for complex geometrical shapes, to include the distortional mode and other possible interaction between the buckling modes. The overall idea of DSM underlies in the use of gross section properties along with the signature curve drawn for all possible half wavelengths of buckling modes. The half wavelengths of short, intermediate and long respectively account for local, distortional and global buckling modes. Thus, it implicitly considers all possible modes in the design. The minimum elastic critical buckling load for the respective modes determined from the signature curve and the gross section properties are input to the semi-empirical DSM design equations to determine the ultimate strength of the compression member. The nominal strength for local, distortional and global modes are

independently determined using respective DSM design equations and the minimum will be the governing nominal strength of the member. The reliability of DSM design is verified for a range of cross-section shapes and those sections are added in AISI specification as prequalified sections but the code permits to extend design for non-prequalified sections by ensuring its reliability index.

The DSM design is meant for the simply supported boundary condition in which the member is allowed to undergo flexural buckling about both the axes and restraint to twisting about the longitudinal axis, whereas warping deformation is allowed and further it is simply supported for local and distortional modes. The other support conditions for the global modes can be accounted using the effective length approach in elastic critical buckling determination and the minimum elastic critical local and distortional modes can be conservatively taken from signature curve. The support condition considered in the experiment allows flexural buckling about minor axis, restraints flexural buckling about major axis and twisting about longitudinal axis, the endplates welded with specimen restraints warping deformation and further provides fixed end condition for the local and distortional modes. The DSM design equations consider the buckling interaction between local and global mode and allows similar approach for distortional and global mode. The residual stress effects, geometrical imperfections, buckling strength, post-buckling strength, interaction between buckling modes and interaction between yielding and buckling are accounted in DSM through the semi-empirical equations. However, the shift in effective centroid is not accounted. The main challenge in upright design using the DSM is to account for perforations. It has been proven that the perforation influence shall be accounted in elastic critical buckling determination using Generalized Beam Theory as initial imperfection. Following which the perforations are rationally accounted in elastic critical buckling determination in terms of effective thickness for the perforated strips. There are literature recommending reduced thickness equations for local, distortional and global modes. The method of implementing the reduced thickness in signature curve may easily account for the perforation in elastic critical buckling determination but its accuracy is solely depending on the recommended reduced thickness value. There are two notable recommendations for reduced thickness equations available in literature to account pattern perforations (Smith and Moen 2014).

4. Results and Discussion

The experimental results show that irrespective of perforations, all the specimens have failed in local mode for the shorter length (L = 580 mm), other unperforated specimens have failed in interactive mode of distortion with flexural buckling about minor axis and other perforated members have failed in interactive mode of local and flexural buckling about minor axis. The introduction of perforation weakens the web element to trigger local bulking, otherwise the web element may offer sufficient stiffness to the flange and rear flange to undergo distortional mode as happened in unperforated members. The perforation width proportionally reduces the ultimate strength and perforation area further reduces the strength for large perforation area. As the member slenderness increases the interaction of local buckling in perforated members subside, however the global mode contribution becomes dominant. The distortional mode participation and its interaction with flexural buckling about minor axis is significant with respect to increase in member slenderness for unperforated members, similar interaction is observed for upright section (Ren et. al. 2019).

Table 4: Experimental and DSM Results

Length ID	L (mm)	Experimental ultimate load P_{u-G} (kN)	Experimental ultimate load P_{u-P1} (kN)	Experimental ultimate load P_{u-P3} (kN)	DSM P_{n-G} (kN)	Method 1 DSM nominal strength $P_{n-P1-M1}$ (kN)	Method 1 DSM nominal strength $P_{n-P3-M1}$ (kN)	Method 2 DSM nominal strength $P_{n-P1-M2}$ (kN)	Method 2 DSM nominal strength $P_{n-P3-M2}$ (kN)
L1	580	76.93	73.04	60.54	76.93	77.67	67.22	73.04	68.35
L2	820	77.63	70.17	64.75	77.63	74.73	67.15	70.17	68.40
L3	1060	77.87	71.85	48.31	77.87	76.47	66.59	71.85	67.46
L4	1300	72.92	59.19	47.97	72.92	73.54	66.25	59.19	67.20
L5	1540	66.77	58.87	41.34	66.77	66.82	66.45	58.87	67.83

Table 5: Comparison of results

Length ID	L (mm)	P_{n-G}/P_{u-G}	$P_{n-P1-M1}/P_{u-P1}$	$P_{n-P1-M2}/P_{u-P1}$	$P_{n-P3-M1}/P_{u-P2}$	$P_{n-P3-M2}/P_{u-P2}$
L1	580	0.82	1.03	0.97	1.11	1.13
L2	820	1.12	1.10	1.03	1.04	1.06
L3	1060	1.12	1.18	1.11	1.38	1.40
L4	1300	0.97	1.17	0.94	1.38	1.40
L5	1540	1.17	1.30	1.15	1.61	1.64
Mean		1.04	1.16	1.04	1.30	1.32

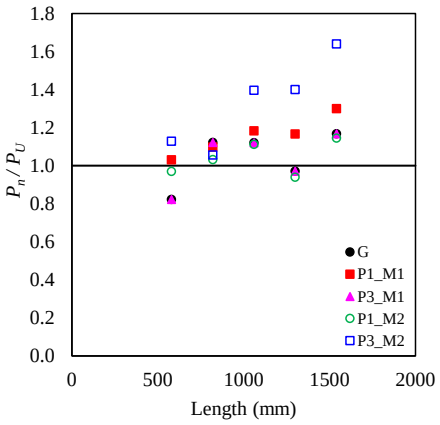

Figure 4: DSM prediction comparison

Direct Strength Method is able to predict the nominal strength precisely for unperforated members, however the reduced thickness equations proposed in literature for accounting perforations may not be able to predict the nominal strength accurately. Among the compared methods, the method 1 (Smith and Moen 2014) treats the perforations using weighted average section properties in elastic global buckling equations which can easily account for various support conditions through effective length factor. Whereas, Method 2 (Casafont et. al. 2012 and Casafont et. al. 2013) uses the finite strip analysis with reduced thickness for perforated strips but with zero applied stress to get global elastic critical buckling stress. Therefore, it is limited to

simply supported boundary condition. In the current study, the members are tested for simply supported only about minor principal axis for which the method 2 may not exhibit the minor axis flexural mode even in higher modes, especially before and near the distortion to global transition region. This can be managed to some extent by constrained finite strip analysis enabled with global mode alone, but it will ignore the contribution of other cross-section buckling modes and resulting in higher elastic critical buckling stress. The method 2 also hinders the usage of generalized beam theory (Bebiano and Camotim 2008) based elastic critical buckling determination in which there is no possibility of applying zero stress for the perforated strips which is the priori for method 2 in elastic critical buckling determination for local, distortional and global modes. The complete equations to determine the nominal strength are presented in Annex 1 and notations involved in the equations are detailed in Annex 2. Both DSM predictions for upright with pattern perforations are not very accurate because the reduced thickness equations might have not accounted the flexural buckling about minor axis immediately after the distortion region in the elastic critical buckling curve. Nominal strengths predicted using DSM is presented in Table 4 and the ratio of DSM nominal strength to experimental ultimate load is presented for all members and both methods of 1 and 2 in Table 5.

Although the method 2 prediction seems to be better, the global critical buckling load for the first three lengths of P1 members are not readily available from its corresponding signature curve, because it exhibits distortional mode for those lengths. Even for the remaining 2 lengths (L4 and L5), the failure mode is flexural-torsional mode and hence the flexural buckling about the minor principal axis is obtained in higher modes of signature curve. Unfortunately, the first three lengths of P1 are unable to deliver elastic critical buckling stress for flexural buckling about minor axis even in higher modes of signature curve. Therefore, constrained finite strip method enabled with global mode alone was done and the flexural buckling about minor axis mode was identified in higher modes. For the P3 perforations, the ratio of overall net perforation width in web element to perforation length is 2 whereas the reduced thickness equations in method 2 are applicable to the same ratio of 1.6. Hence the method 2 DSM predictions are not applicable for P3 perforation type. The mean value of the strength ratio is accurate for perforated members having P1 pattern compared to P3. Fig. 6 compares the accuracy of the DSM predictions with reference to experimental results and it is observed that most of the predicted strengths are higher than experimental results and thus finds place above the P_n/ P_u ratio equal to one in the graph. Both the methods may imply better nominal strength at least for P1 perforation when the interaction between distortion and global mode is accounted, however the experimental results clearly indicates that the failure mode is having the interaction between local and global modes. The accuracy of both the methods can be further improved by including the effective shift in centroid and for the same the presented experimental results will add value. Including those results in effective thickness calculation can possibly avoid the over estimation of nominal strength in DSM design. Since both the methods are unable to predict the correct failure mode it shouts immediate attention for accurate DSM design considering pattern perforations in the view of perforation size, shape and support conditions. However, the inaccuracy of Method 2 in predicting the local mode is reported and seeks further improvement.

5. Conclusions

The behavior of simple rack upright having pattern perforation subject to axial compression is experimentally investigated for the end support condition of simply supported only about minor

principal axis. The experimental results clearly evident that the presence of perforation can alter the contributing mode of failure from distortion of unperforated member to local. Therefore, for the small perforations the interaction of distortional mode with flexural buckling about minor axis is non-negligible in the upright frames and hence this interaction should be accounted in the design. Large perforation dimension oriented along the transverse direction exceedingly lowers the ultimate strength when compared with its orientation along member length. The small size perforations, oriented with small perforation dimension along the transverse direction can enhance the member capacity. Possibly the data used in the derivation of effective thickness might have not accounted effective centroid shift in both experiment results and numerical predictions. Accounting this shift in effective thickness calculation may result the accurate nominal strength and failure mode.

Appendix 1: DSM Design Equations

Yielding and Global Buckling

$$P_y = A_g F_y \tag{1}$$

$$P_{ne} = \left(0.658^{\lambda_c^2}\right) P_y \text{ for } \lambda_c \le 1.5 \tag{2}$$

$$P_{ne} = \left(\frac{0.877}{\lambda_c^2}\right) P_y \text{ for } \lambda_c > 1.5 \tag{3}$$

$$\lambda_c = \sqrt{\frac{P_y}{P_{cre}}} \tag{4}$$

Elastic critical flexural buckling load

$$P_{cre} = \frac{\pi^2 EI}{\left(KL\right)^2} \tag{5}$$

Method 1- Elastic critical buckling load

$$P_{cre} = P_{cre,f,nh} \frac{I_{avg}}{I_g} \tag{6}$$

$$I_{avg} = \frac{I_g L_g + I_{net} L_{net}}{L} \tag{7}$$

$$P_{cre,f,nh} = \frac{\pi^2 EI_g}{L^2} \tag{8}$$

$$L_{net} = n_l L_h \tag{9}$$

$$L_g = L - L_{net} \tag{10}$$

Method 2 - Reduced thickness equation for global mode

$$t_{rG} = 0.7t\left(\frac{L_{np}}{L}\right) \tag{11}$$

Local Buckling

Members without holes

$$P_{nl} = P_{ne} \quad for \;\; \lambda_l \le 0.776 \tag{12}$$

$$P_{nl} = \left[1 - 0.15\left(\frac{P_{crl}}{P_{ne}}\right)^{0.4}\right]\left(\frac{P_{crl}}{P_{ne}}\right)^{0.4} P_{ne} \quad for \quad \lambda_l > 0.776, \tag{13}$$

$$\lambda_l = \sqrt{\left(\frac{P_{ne}}{P_{crl}}\right)} \tag{14}$$

Members with Holes

$$P_{nl} \le P_{ynet} \tag{15}$$

$$P_{ynet} = A_{net} F_y \tag{16}$$

Method 1 - Reduced thickness equation for local

$$t_{rL} = t\left[1 - \frac{n_l n_t \left(L_h d_h + \mu d_h \alpha + \mu L_h \beta + \alpha\beta\right)}{Lb}\right]^{1/2} \tag{17}$$

Method 2 - Reduced thickness equation for local

$$t_{rL} = 0.61t\frac{L_{np}B_{np}}{LH} + 0.18t\frac{B_p}{L_p} + 0.11 \tag{18}$$

Distortional Buckling

Members without holes

$$P_{nd} = P_y \quad for \quad \lambda_d \le 0.561 \tag{19}$$

$$P_{nd} = \left[1 - 0.25\left(\frac{P_{crd}}{P_y}\right)^{0.6}\right]\left(\frac{P_{crd}}{P_y}\right)^{0.6} P_y \quad for \quad \lambda_d > 0.561 \tag{20}$$

$$\lambda_d = \sqrt{\left(\frac{P_y}{P_{crd}}\right)} \tag{21}$$

$$P_y = A_g F_y \tag{22}$$

Members with holes

$$P_{nd} = P_{ynet} \quad for \quad \lambda_d \le \lambda_{d1} \tag{23}$$

$$P_{nd} = P_{ynet} - \left(\frac{P_{ynet} - P_{d2}}{\lambda_{d2} - \lambda_{d1}} \right) \left(\lambda_d - \lambda_{d1} \right) \quad for \quad \lambda_{d1} < \lambda_d \le \lambda_{d2} \tag{24}$$

$$\lambda_d = \sqrt{\frac{P_y}{P_{crd}}} \tag{25}$$

$$\lambda_{d1} = 0.561 \left(\frac{P_{ynet}}{P_y} \right) \tag{26}$$

$$\lambda_{d2} = 0.561 \left[14.0 \left(\frac{P_y}{P_{ynet}} \right)^{0.4} - 13.0 \right] \tag{27}$$

$$P_{d2} = \left[1 - 0.25 \left(\frac{1}{\lambda_{d2}} \right)^{1.2} \right] \left(\frac{1}{\lambda_{d2}} \right)^{1.2} P_y \tag{28}$$

$$P_y = A_g F_y \tag{29}$$

$$P_{ynet} = A_{net} F_y \tag{30}$$

Method 1 - Reduced thickness equation for distortional mode

$$t_{rD} = t \left(\frac{A_{web,net}}{A_{web,g}} \right)^{1/3} \tag{31}$$

Method 2 - Reduced thickness equation for distortional mode

$$t_{rD} = 0.9t \left(\frac{L_{np}}{L} \right)^{1/3} \tag{32}$$

Appendix 2: Nomenclature

A_g	-	Gross area of cross-section
A_{net}	-	Net area of cross-section at the location of a hole
$A_{web,g}$	-	Planar gross area of the web
$A_{web,net}$	-	Planar net area of the web
b	-	Width of stiffened element
B_{np}	-	Width of non-perforated strip
B_p	-	Total width of perforations
d_h	-	Width of perforation
E	-	Modulus of elasticity of steel
F_{cre}	-	Critical elastic (flexural) buckling stress
F_n	-	Nominal compressive stress
F_y	-	Yield stress

H	-	Total Flange Length
I_{avg}	-	Weighted average moment of inertia about the axis of buckling
I_g	-	Moment of inertia of gross cross-section about axis of buckling
I_{net}	-	Moment of inertia of net cross-section about axis of buckling
K	-	Effective length factor
L	-	Pitch Length, Length of the member
L_g	-	Segment length without holes
L_h	-	Length of perforation
L_{net}	-	Length of net cross-section
L_{np}	-	Length of nonperforated sheet between perforations
L_p	-	Length of perforation
n_l	-	Number of rows of fasteners spaced longitudinally
n_t	-	Number of rows of fasteners spaced transversely
P_{crd}	-	Distortional buckling force(load)
P_{cre}	-	Global buckling force
P_{crl}	-	Local buckling force(load)
P_{d2}	-	Nominal axial strength[resistance] of distortional buckling at λ_{d2}
P_{nd}	-	Nominal axial strength for distortional buckling
P_{ne}	-	Nominal axial strength [resistance] for overall buckling
P_{nl}	-	Nominal axial strength [resistance] for local buckling
$P_{cre,f,nh}$	-	Critical elastic flexural buckling load of the unperforated member
P_y	-	Member axial yield strength
P_{ynet}	-	Member yield strength on net cross-section
r	-	Radius of gyration of full unreduced cross-section about the axis of buckling
t	-	Actual Thickness
t_{rD}	-	Reduced thickness for distortional buckling
t_{rG}	-	Reduced thickness for global buckling
t_{rL}	-	Reduced thickness for local buckling
α	-	Perforation dimension modification factor for the longitudinal direction
β	-	Perforation dimension modification factor for the transverse direction
μ	-	Poisson's ratio of material

References

AISI-S100 (2016). "North American specification for the Design of Cold-Formed Steel Structural Members, American Iron and Steel Institute", *AISI*, Washington, DC.

Baldassino, N., Bernuzzi, C., Gioia, A.D., Simoncelli, M., (2019). "An Experimental Investigation on Solid and Perforated Steel Storage Racks Uprights." *Journal of Constructional Steel Research,* 155 409–425.

Bebiano, R., Silvestre, N., Camotim, D., (2008). "GBTUL - A Code for the Buckling Analysis of Cold-Formed Steel Members." *19th International Specialty Conference on Cold-Formed Steel Structures,* St. Louis, Missouri, U.S.A. 61–79.

Casafont, M., Pastor, M.M., Roure, F., Peköz, T., (2011). "An Experimental Investigation of Distortional Buckling of Steel Storage Rack Columns." *Thin-Walled Structures*, 49(8) 933–946.

Casafont, M., Pastor, M., Bonada, J., Roure, F., Peköz, T., (2012). "Linear Buckling Analysis of Perforated Steel Storage Rack Columns with the Finite Strip Method." *Thin-Walled Structures*, 61 71–85.

Casafont, M., Pastor, M.M., Roure, F., Bonada, J., Peköz, T., (2013). "Design of Steel Storage Rack Columns via the Direct Strength Method." *Journal of Structural Engineering*, 139(5) 669-679

Davies, J.M., Leach, P., Taylor, A., (1997). "The Design of Perforated Cold-Formed Steel Sections Subject to Axial Load and Bending." *Thin-Walled Structures* 29(1–4) 141–157

European committee for Standardization (2009), steel Static Storage systems- Adjustable pallet racking systems-Principles for structural design" *EN 15512*, Brussels, Belgium

Li, Z., Schafer, B.W., (2010). "Buckling Analysis of Cold-Formed Steel Members with General Boundary Conditions Using CUFSM: Conventional and Constrained Finite Strip Methods." *20th International Specialty Conference on Cold-Formed Steel Structures*, St. Louis, Missouri, U.S.A. 17–31.

Moen, C.D., (2008). "Direct Strength Design of Cold-Formed Steel Members with Perforations". PhD Dissertation. *The Johns Hopkins University*, Baltimore, 529.

Moen, C.D., Schafer, B.W., (2008). "Experiments on Cold-Formed Steel Columns with Holes." *Thin-Walled Structures* 46(10) 1164–1182.

Moen, C.D., Schafer, B.W., (2009). "Elastic Buckling of Cold-Formed Steel Columns and Beams with Holes." *Engineering Structures* 31(12) 2812–2824.

Moen, C.D., Schafer, B.W., (2011). "Direct Strength Method for Design of Cold-Formed Steel Columns with Holes." *Journal of Structural Engineering* 137(5) 559–570.

Ren, C., Wang, B., Zhao, X., (2019). "Numerical Predictions of Distortional-Global Buckling Interaction of Perforated Rack Uprights in Compression." *Thin-Walled Structures* 136 292–301.

Rhodes, J., Schneider, F.D., (1994). "The Compressional Behaviour of Perforated Elements." *12th International Specialty Conference on Cold-Formed Steel Structures*, St. Louis, Missouri, U.S.A. 11–28.

Rhodes, J., Macdonald, M., (1996). "The Effects of Perforation Length on the Behaviour of Perforated Elements in Compression." *13th International Specialty Conference on Cold-Formed Steel Structures*, St. Louis, Missouri, U.S.A. 91-101.

RMI. (2012). Specification for the Design, Testing and Utilization of Industrial Steel Storage Racks. *Rack Manufacturers Institute*, Rack Manufacturers Institute.

Roure, F., Pastor, M.M., Casafont, M., Somalo, M.R., (2011). "Stub Column Tests for Racking Design: Experimental Testing, FE Analysis and EC3." *Thin-Walled Structures* 49(1) 167–184.

Schafer, B. (2006). "Direct Strength Method (DSM) Design Guide". Design Guide CF06-1, *American Iron and Steel Institute.*

Schafer, B.W., Adany, S., (2006). "Buckling Analysis of Cold-Formed Steel Members Using CUFSM: Conventional and Constrained Finite Strip Methods." *18th International Specialty Conference on Cold-Formed Steel Structures*, Orlando, Florida

Smith, F.H., Moen, C.D., (2014). "Finite Strip Elastic Buckling Solutions for Thin-Walled Metal Columns with Perforation Patterns." *Thin-Walled Structures* 79 187–201.

Trouncer, A. N., and Rasmussen, K. J. R. (2014a). Flexural–torsional buckling of ultra light-gauge steel storage rack uprights. *Thin-Walled Structures*, 81, 159–174.

Trouncer, A. N., and Rasmussen, K. J. R. (2014b). Flexural–torsional buckling of ultra light-gauge steel storage rack uprights. *Thin-Walled Structures*, 81, 159–174.

VijayaVengadesh Kumar, J., and Arul Jayachandran, S. (2016). "Experimental investigation and evaluation of Direct Strength Method on beam-column behavior of uprights". *Thin-Walled Structures*, 102, 165–179.

Young, B., and Rasmuseen J. R., (1998), "Design of Lipped Channel Columns*." Journal of Structural Engineering, ASCE*, 124 140-148.

Yu, W.-W., and LaBoube, R. A. (2010). "Cold-Formed Steel Design: Fourth Edition. Cold-Formed Steel Design: Fourth Edition", *John Wiley and Sons*, Missouri University of Science and Technology, Rolla, MO, United States.